Supplementary Information

Efficient stepwise carrier concentration optimization in $Ge_{(1+x)-y}Sb_yTe$

Wan-Yu Lyu,[a] Wei-Di Liu,[a,*] Meng Li,[a] Xiao-Lei Shi,[a] Min Hong,[b] Wenyi Chen,[c] Tianyi Cao,[a] Boxuan Hu,[a] Yongqi Chen,[a] Kai Guo,[d,] Zhi-Gang Chen[a,*]

[a]School of Chemistry and Physics, ARC Research Hub in Zero-emission Power Generation for Carbon Neutrality, and Centre for Materials Science, Queensland University of Technology, Brisbane, QLD 4000.

[b]Centre for Future Materials, University of Southern Queensland, Springfield, Queensland 4300, Australia.

[c]School of Mechanical and Mining Engineering, The University of Queensland, Brisbane, Queensland 4072, Australia.

[d]School of Physics and Materials Science, Guangzhou University, Guangzhou 510006, China

Email: zhigang.chen@qut.edu.au; weidi.liu@qut.edu.au

1. Experimental section

1.1 Synthesis

Polycrystalline samples were prepared in the composition of $Ge_{(1+x)-y}Sb_yTe$ (x=0, 0.02, 0.04, 0.06, 0.08; y=0.04, 0.06, 0.08, 0.12). Precursors, including Ge (99.999%, Sigma-Aldrich, Australia), Te (99.999%, Sigma-Aldrich, Australia), Sb (99.999%, Alfa-Aesar, United States), were weighed following the nominal compositions. The weighted precursors were sealed in quartz ampules and heated in 1223 K for 24 hours followed by water quenching. The obtained samples were further annealed at 873 K for 3 days. The resultant products were further ground into powders and sintered into pellets (SPS, 70 Mpa and 723K) for performance measurement.

1.2 Characterization

The crystal structures of as-prepared samples were characterized by X-ray diffraction (XRD, Bruker, United States, Cu K_α radiation with a wavelength of 1.5418 Å, $10° \leq 2\theta \leq 80°$, step with 0.02°). Field-emission scanning electron microscope (FE-SEM, JSM-7100F, JEOL, Japan) equipped with energy dispersive spectrum (EDS) detector was employed to explore the morphologies and compositions.

1.3 Thermoelectrical Property Measurement

S (Seebeck coefficient) and σ (electrical conductivity) of the sintered pellets were simultaneously measured by ZEM-3 (ULVAC Technologies, Inc., Japan). κ_{total} (total thermal conductivity) is calculated by $\kappa_{total}=D\times C_p\times\rho$, where C_p is the specific heat estimated from the Dulong-Petit approximation [1], ρ is the pellet densities measured by Archimedes method, and D is the thermal diffusivity coefficient measured by the laser flash diffusivity apparatus (LFA 467, Netzsch, Gemany). The Hall coefficient (R_H) was measured based on Van der Paw technique [2]. The n_p (hole concentration) and hole mobility (μ_p) were through the equation $n_p=1/(eR_H)$ and $\mu_p=\sigma R_H$, where e is the electron charge.

2. Thermoelectric properties of $Ge_{(1+x)}Te$.

Figure S1 displays the thermoelectric properties of $Ge_{(1+x)}Te$ (x=0, 0.02, 0.04, 0.06, 0.08). **Figure**

S1a shows the electrical conductivity (σ) of $Ge_{(1+x)}Te$ (x=0, 0.02, 0.04, 0.06, 0.08). σ decrease with increased Ge content due to reduced carrier concentration (n_p). on the contrary, Seebeck coefficient (S) increases with increased Ge content, as shown in **Figure S1**b. In this way, combining these two coupled effect on electrical properties, the power factor ($S^2\sigma$) was displayed in **Figure S1**c. The enlarged $S^2\sigma$ was obtained with the composition of $Ge_{1.04}Te$. Total thermal conductivity (κ_{tot}) of $Ge_{(1+x)}Te$ (x=0, 0.02, 0.04, 0.06, 0.08) are shown in **Figure S1**d. The κ_{tot} increase with increased Ge content. **Figure S1**e shows the electronic thermal conductivity (κ_e) of $Ge_{(1+x)}Te$ (x=0, 0.02, 0.04, 0.06, 0.08). κ_e is calculated following the Wiedemann−Franz law formula, $\kappa_e=L\sigma T$, where L is the Lorenz number, σ represents the electrical conductivity, and T is the absolute temperature. The L is calculated using the following equation proposed by Kim *et al*. based on single parabolic band assumption [3]: $L = 1.5 + exp\frac{-|S|}{116}$, where S is the Seebeck coefficient. κ_e decrease with increased Ge content from GeTe to $Ge_{1.08}Te$. The lattice thermal conductivity (κ_l) is estimated by deducting κ_e from measured κ_{tot}: $\kappa_l=\kappa_{tot}-\kappa_e$. The results shown in **Figure S1**f. κ_l increases with increased Ge content. This may be due to the increased Ge precipitates in the GeTe matrix. The extra-matrix Ge exists as composites, the increased composites content resulting in enlarged κ_l.

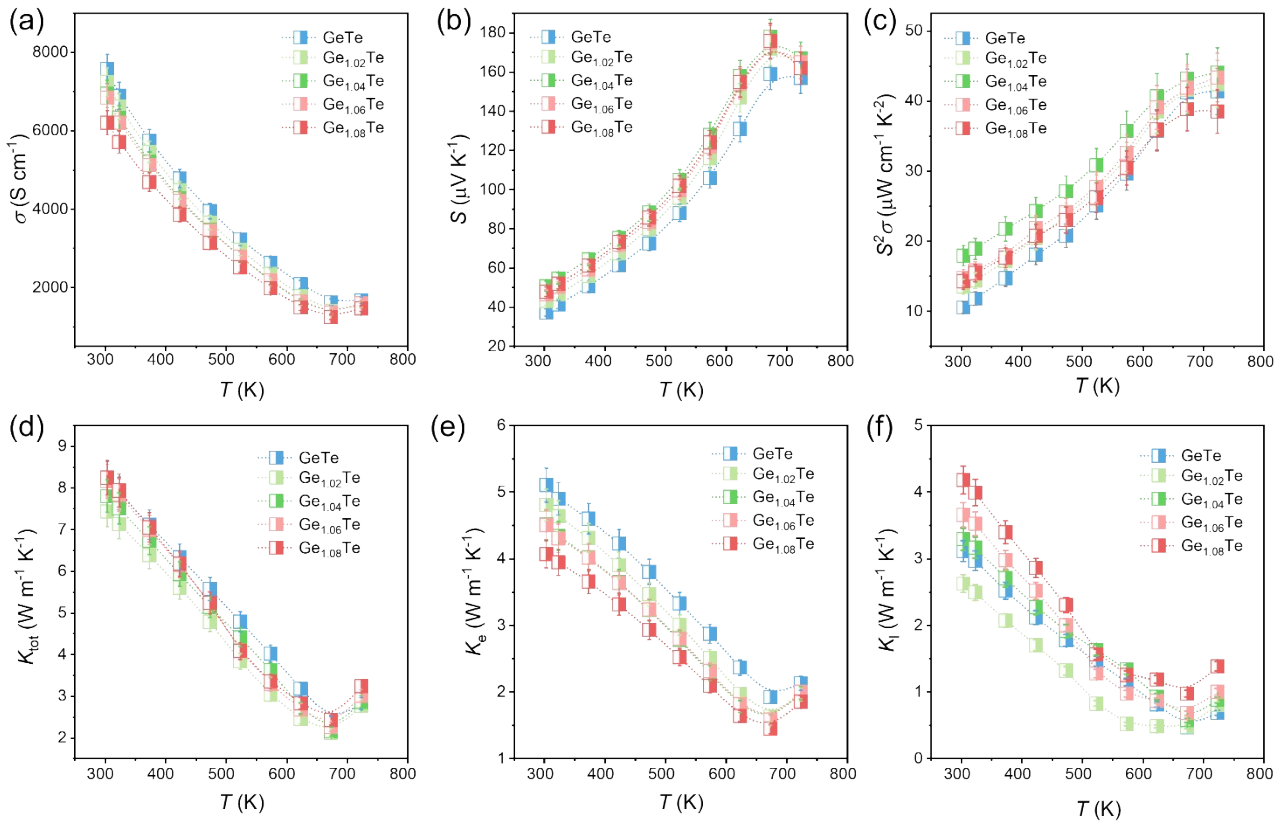

Figure S1. Electrical and thermal properties of $Ge_{(1+x)}Te$ (x=0, 0.02, 0.04, 0.06, 0.08). The temperature-dependent (a) σ, (b) S, (c) $S^2\sigma$, (d) κ_{tot}, (e) κ_e, and (f) κ_l.

Figure S2 shows the zT value of $Ge_{(1+x)}Te$ (x=0, 0.02, 0.04, 0.06, 0.08). Due to the contribution of both electrical and thermal parts, peak zT of 1.35 was achieved with $Ge_{1.04}Te$ at 673K.

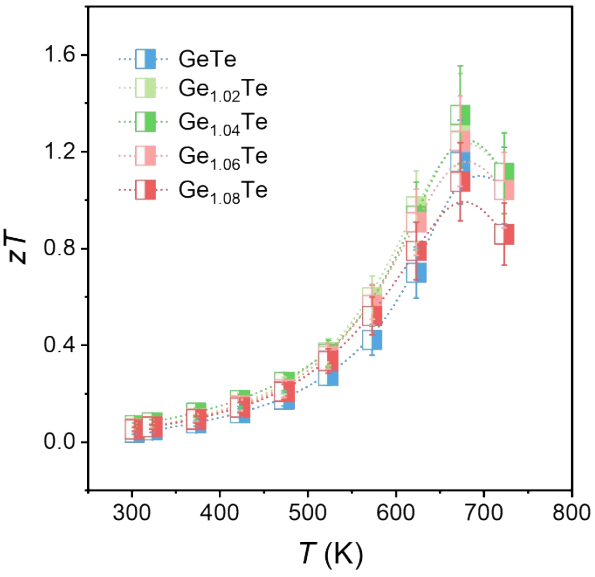

Figure S2. zT value of $Ge_{(1+x)}Te$ (x=0, 0.02, 0.04, 0.06, 0.08).

Figure S3 displays the enlarged peak of Ge precipitates of all samples.

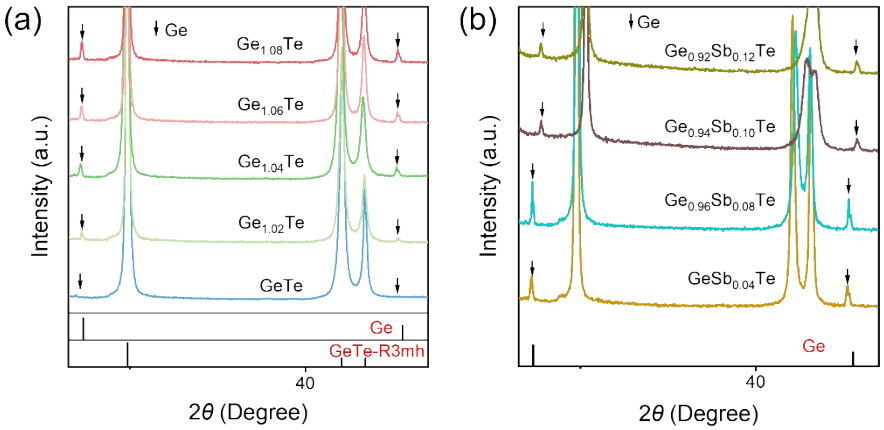

Figure S3. Enlarged peak of Ge precipitates for (a) $Ge_{(1+x)}Te$ (x=0, 0.02, 0.04, 0.06, 0.08), and (b) $Ge_{1.04-y}Sb_yTe$ (y=0.04, 0.08, 0.10, 0.12).

Figure S4 shows the comparation of zT values with other Sb single doped GeTe. The zT value of $Ge_{1.96}Sb_{0.08}Te$ is comparable to the literatures.

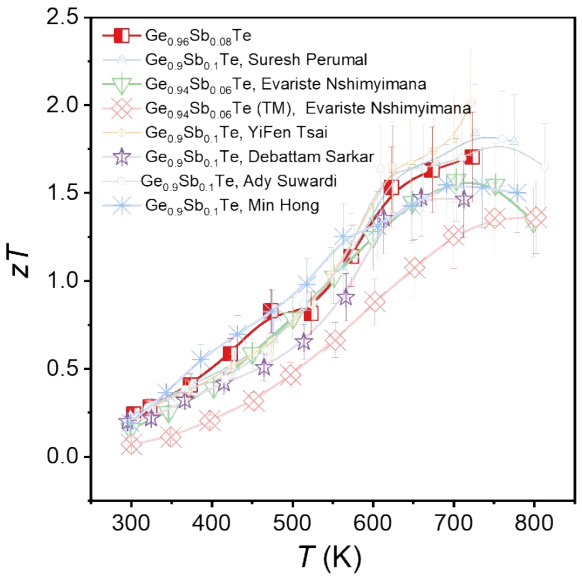

Figure S4. Comparation of zT values with other Sb single doped GeTe.

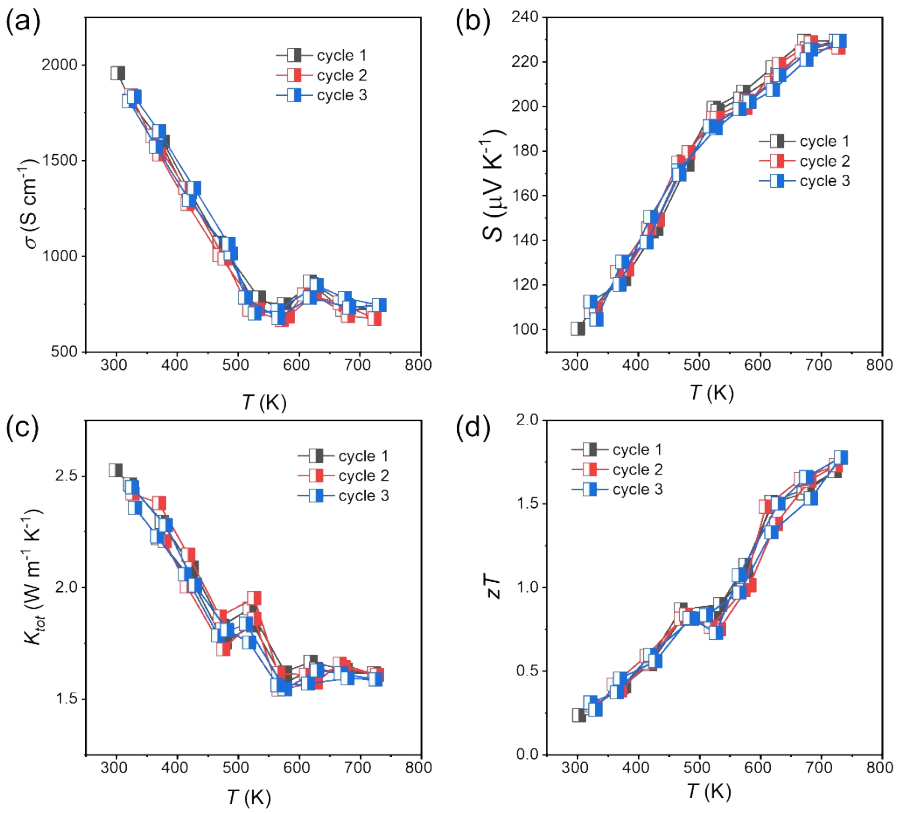

Figure S5. 3 Cycling test of thermoelectric properties for $Ge_{0.96}Sb_{0.08}Te$.

3. Electrical transport properties

The determination of effective mass m^* in this work is based on the single parabolic band (SPB) approximation with the acoustic phonon scattering [4, 5].

$$m^* = \frac{h^2}{2k_BT}\left[\frac{n}{4\pi F_{1/2}(\eta)}\right]^{2/3} \tag{1}$$

$$S = \pm\frac{k_B}{e}\left(\frac{2F_1(\eta)}{F_0(\eta)} - \eta\right) \tag{2}$$

$$F_n(\eta) = \int_0^\infty \frac{x^n dx}{1 + e^{x-\eta}} \tag{3}$$

$$\eta = \frac{E_f}{k_BT} \tag{4}$$

Where k_B is the Boltzmann constant, e the electron charge, h the Planck constant, E_f is the Fermi

energy, η is the reduced Fermi energy, $F_n(\eta)$ is the n-th order Fermi integral. Based on the measured room temperature Seebeck coefficient (S) and carrier concentration (n), m^* can then be determined from equation (1-4)."

Table S1. The carrier concentration (n_p), carrier mobility (μ_p), and mass density of all samples.

Composition	n_p (10^{20} cm^{-3})	μ_p (cm^2 V^{-1} s^{-1})	ρ (g cm^{-3})
GeTe	8.23	57.44	5.9352
$Ge_{1.02}Te$	7.52	60.15	5.8968
$Ge_{1.04}Te$	6.83	63.48	5.946
$Ge_{1.06}Te$	4.53	94.35	5.8645
$Ge_{1.08}Te$	3.84	100.87	5.8974
$GeSb_{0.04}Te$	3.22	52.52	5.8245
$Ge_{0.96}Sb_{0.08}Te$	2.78	44.32	5.9838
$Ge_{0.94}Sb_{0.10}Te$	2.36	20.96	5.8744
$Ge_{0.92}Sb_{0.12}Te$	1.83	10.54	5.8326

4. Thermal transport properties

Element substitution can cause lattice fluctuation and led to a disorder of the crystal matrix, which can be expressed by the Callaway [6] and Klmen [7] model, which has been used by many thermoelectric systems [8-10]. The lattice distribution can be evaluated by κ_l/κ_{l0}, which κ_{l0} represents the lattice thermal conductivity of pristine GeTe, κ_l is measured lattice thermal conductivity of $Ge_{(1+x)-y}Sb_yTe$.

$$\frac{\kappa_l}{\kappa_{l0}} = \frac{\tan^{-1}(u)}{u} \tag{5}$$

$$u^2 = \frac{\pi^2 \theta_D \Omega}{h v_s^{\ 2}} \kappa_{l0} \Gamma_{tot} \tag{6}$$

where u, Ω, v_s, θ_D, and Γ_{tot} are the disorder scaling parameter, the average volume per atom, the sound

velocity, the Debye temperature, and the experimental disorder scattering parameter, respectively. Γ_{tot} can be derived from measured κ_l.

Reference

1. J. Li, X. Y. Zhang, S. Q. Lin, Z. W. Chen and Y. Z. Pei, *Chemistry of Materials*, 2017, **29**, 605-611.
2. K. A. Borup, E. S. Toberer, L. D. Zoltan, G. Nakatsukasa, M. Errico, J.-P. Fleurial, B. B. Iversen and G. J. Snyder, *Rev. Sci. Instrum.*, 2012, **83**.
3. H.-S. Kim, Z. M. Gibbs, Y. Tang, H. Wang and G. J. Snyder, *APL Materials*, 2015, **3**.
4. H. J. Goldsmid, *Introduction to Thermoelectricity*, Springer Series in Materials Science, 2016.
5. J. Zhu, X. Zhang, M. Guo, J. Li, J. Hu, S. Cai, W. Cai, Y. Zhang and J. Sui, *npj Computational Materials*, 2021, **7**.
6. J. Callaway and H. C. von Baeyer, *Phys. Rev.*, 1960, **120**, 1149-1154.
7. P. G. Klemens, *Phys. Rev.*, 1960, **119**, 507-509.
8. J. Yang, G. P. Meisner and L. Chen, *Appl. Phys. Lett.*, 2004, **85**, 1140-1142.
9. H. Wang, A. D. LaLonde, Y. Pei and G. J. Snyder, *Adv. Funct. Mater.*, 2013, **23**, 1586-1596.
10. Z. Zheng, X. L. Su, R. G. Deng, C. Stoumpos, H. Y. Xie, W. Liu, Y. G. Yan, S. Q. Hao, C. Uher, C. Wolverton, M. G. Kanatzidis and X. F. Tang, *J. Am. Chem. Soc.*, 2018, **140**, 2673-2686.